

Magnetoacoustic sensing of magnetic nanoparticles

Stephan Kellnberger,^{1,2,3} Amir Rosenthal,^{2,3,4} Ahne Myklatun,^{3,5}
Gil Westmeyer,^{3,5,6} George Sergiadis,⁷ and Vasilis Ntziachristos^{2,3}

¹*Cardiovascular Research Center, Cardiology Division,
Massachusetts General Hospital, Harvard Medical School,
185 Cambridge St, Boston, Massachusetts 02114, USA*

²*Chair for Biological Imaging, Technische Universität München, Trogerstraße 9, 81675 München, Germany*

³*Institute for Biological and Medical Imaging, Helmholtz Zentrum München,
Ingolstädter Landstraße 1, 85674 München, Germany*

⁴*Andrew and Erna Viterbi Faculty of Electrical Engineering,
The Technion - Israel Institute of Technology, Haifa 32000, Israel*

⁵*Institute of Developmental Genetics (IDG), Helmholtz Zentrum München,
Ingolstädter Landstraße 1, 85674 München, Germany*

⁶*Department of Nuclear Medicine, Technische Universität München, Ismaninger Str. 22, 81675 München, Germany*

⁷*Department of Electrical and Computer Engineering,
Aristotle University, Egnatia Str., 54124 Thessaloniki, Greece*

The interaction of magnetic nanoparticles and electromagnetic fields can be determined through electrical signal induction in coils due to magnetization. However, the direct measurement of instant electromagnetic energy absorption by magnetic nanoparticles, as it relates to particle characterization or magnetic hyperthermia studies, has not been possible so far. We introduce the theory of magnetoacoustics, predicting the existence of second harmonic pressure waves from magnetic nanoparticles due to energy absorption from continuously modulated alternating magnetic fields. We then describe the first magnetoacoustic system reported, based on a fiber-interferometer pressure detector, necessary for avoiding electric interference. The magnetoacoustic system confirmed the existence of previously unobserved second harmonic magnetoacoustic responses from solids, magnetic nanoparticles, and nanoparticle-loaded cells, exposed to continuous wave magnetic fields at different frequencies. We discuss how magnetoacoustic signals can be employed as a nanoparticle or magnetic field sensor for biomedical and environmental applications.

PACS numbers: 78.20.Pa, 87.50.C-, 87.50.S-, 43.35.Ud

Electromagnetic (EM) field interaction with magnetic nanoparticles is exploited in many biomedical applications. Magnetic resonance imaging (MRI) employs particles with magnetic properties placed under strong magnetic fields to impart contrast by altering predominantly T2-relaxation times [1–3]. Magnetomotive (mm) based imaging methods such as mm-ultrasound (US) or mm-optical coherence tomography measure the local displacement of nanoparticle labeled tissue based on US signals or altered optical scattering due to introduced magnetic nanoparticles [4, 5]. Magnetic particle imaging (MPI) visualizes the non-linear magnetization response of superparamagnetic iron-oxide nanoparticles driven by a modulated EM field [6]. Magnetic nanoparticles under continuous wave (CW) electromagnetic energy generate heat and are employed in hyperthermia [7, 8] for treating tumors [9, 10]. At more moderate energy depositions, heating mechanisms have been utilized in actuating cell functions [11–13] or remotely triggering drug release [14, 15]. Transient heating of matter is associated with the generation of sound waves using the photoacoustic effect [16, 17]. It has been postulated that it would be possible to generate acoustic waves from magnetic nanoparticles [18] and conducting objects [19] during abrupt on and off transitions of magnetic field bursts. These studies assumed that acoustic waves are not present when employing CW field excitation [18, 19]. Magnetoacoustic

responses have been previously demonstrated but with a frequency identical to the carrier frequency of the excitation field [20, 21]. We have previously demonstrated that second harmonic acoustic signals are generated from conductive media in response to intermittent RF-fields [22]. However, the generation of second harmonic responses to CW-fields has not been shown. Likewise there has been no confirmation or knowledge of the relation of magnetic field strength and resulting second harmonic responses from a magnetic medium.

In this work, we disprove early hypotheses by theoretically establishing and experimentally demonstrating acoustic signal induction in the MHz range, generated by magnetic nanoparticles placed within CW magnetic fields. We conclusively demonstrate that such responses are non-linear, emitting second-harmonic ultrasonic sound waves. To validate the results and reject electromagnetic interference signals that could bias the measurements, we employed an optical pulse interferometer [23], which offered proof of the existence of second harmonic sound waves from magnetic particles in solution or in a biological environment.

Results

Magnetoacoustics is understood in the context of a thermodynamic system comprised of a magnetic medium

[18, 24], by employing the first law of thermodynamics

$$dU = \delta Q + \delta W \quad (1)$$

where Q is the added heat in a closed thermodynamic system, W is the exerted work on the system, and U is the internal energy represented by the kinetic and potential energies of all particles that interact within the system, including also Néel and Brownian relaxation (see Supplemental Material [25]). If the magnetic medium is exposed to alternating magnetic fields (AMF), the differential magnetic work exerted on the system can be described by $\delta W = \vec{H} \cdot d\vec{B}$ with \vec{H} being the magnetic field intensity and \vec{B} the magnetic induction, i.e. $B = \mu_0(H + M)$ where M represents the magnetization and μ_0 is the permeability of free space. Assuming adiabatic conditions, i.e. that no heat is added externally to the magnetic fluid ($\delta Q = 0$), the internal energy is simplified to

$$\frac{dU}{dt} = \mu_0 H \left(\frac{dH}{dt} + \frac{dM}{dt} \right). \quad (2)$$

We can now consider an alternating magnetic field $H(t) = H_0 \cos(\omega_0 t)$ of amplitude H_0 and angular frequency $\omega_0 = 2\pi f_{RF}$, and assume a resulting magnetization of the magnetic medium $M(t) = H_0(\chi' \cos(\omega_0 t) + \chi'' \sin(\omega_0 t))$ where χ' is the real component and χ'' is the imaginary component of the complex magnetic susceptibility χ . Then, we can derive the internal energy U of our magnetic medium due to magnetization evoked by a continuous EM wave, i.e.

$$\begin{aligned} \frac{dU}{dt} = & \frac{1}{2} \mu_0 \omega_0 H_0^2 \{ -(1 + \chi') \sin(2\omega_0 t) \\ & + \chi'' [1 + \cos(2\omega_0 t)] \}. \end{aligned} \quad (3)$$

Eq. (3) describes the power dissipation density in the magnetic medium due to magnetic field heating and exhibits the appearance of second harmonic resonances. Calculating the time integral of Eq. (3) yields the energy deposition density $Q_{MNP}(t) = \int_{t_1}^{t_{end}} U(t) dt$, $t_{end} = n \cdot 2\pi/\omega_0$, $n \in \mathbb{R}$ which can be used to determine the local pressure rise within the magnetic fluid

$$p_0(t) = \frac{\beta}{\kappa \rho C_v} Q_{MNP}(t), \quad (4)$$

where β is the thermal coefficient of volumetric expansion, κ the isothermal compressibility, ρ the mass density, and C_v the volumetric heat capacity. Eq. (4) reflects the proportionality of induced magnetoacoustic pressure waves to the deposited energy as a function of $2\omega_0$. We note that previous studies have failed to report the presence of responses to CW excitation in general [16,17] and the appearance of second harmonic responses in particular, because they assumed integration over full magnetic field cycles 2π resulting in a time independent energy deposition density $Q_{MNP,2\pi} = \int_t^{t+2\pi/\omega_0} U(t) dt = \mu_0 \pi \chi'' H_0^2$.

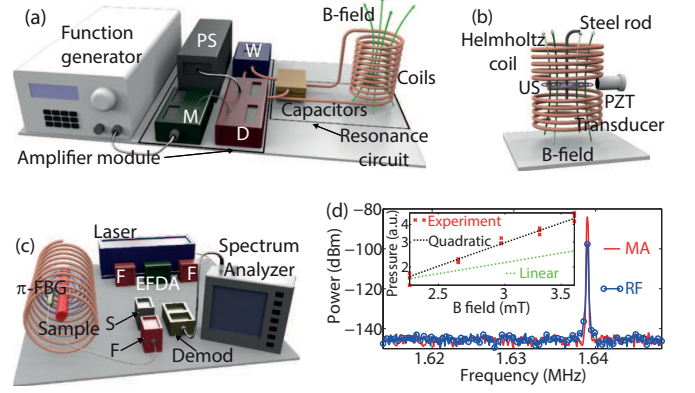


FIG. 1. Concept of magnetoacoustic signal induction. (a) Components of the magnetoacoustic setup. PS - power supply, M - modulator, W - water chiller, D - driver. (b) Magnetoacoustic sensing using a PZT transducer. The sample comprises a steel rod located within the coil. (c) RF-free magnetoacoustic sensing employing a fiber-Bragg-based interferometric ultrasound sensor in a horizontally arranged solenoid (water tank not displayed). The optical sensor comprises optical filters (F), an erbium-doped fiber amplifier (EFDA), a 99/1 optical splitter (S), a demodulator (Demod), and the π -shifted FBG sensing unit. (d) Magnetoacoustic sensing of a steel rod specimen using PZT based ultrasound detection. RF-interference due to the non-linearity of the RF amplifier (blue dotted line) and experimental confirmation of the second harmonic magnetoacoustic signal (red line) induced in conducting material at $f_{MA} = 2f_{RF}$. Inset shows the quadratic increase of detected magnetoacoustic signal (red crosses) as a function of linearly rising B -field compared to the expected theory (dashed black curve) and a linear relationship (dotted green line).

Platform design and magnetoacoustic signal detection.

As a next step, we aimed to validate our theoretical findings in Eq. (4). Since there has been no documented measurement of magnetoacoustic signals, in either the pulsed or CW regimes, a first major goal in this work was to experimentally prove the existence of magnetoacoustic signals. Then, a second goal was to prove Eq. (4), i.e. that magnetic media emit second harmonic magnetoacoustic signals in response to continuous excitation waves. To investigate our hypotheses we designed the first reported magnetoacoustic system, based on a generator of CW magnetic fields [35, 36], and fiber-based interferometric detection (Fig. 1). The system utilized a home-built signal generator ($f_{RF} < 2$ MHz, $B < 12$ mT) driving different types of solenoids to couple energy to the specimen. Samples comprised conductive elements such as a steel rod and different magnetic fluids injected in a polyvinyl chloride (PVC) tubing ($\varnothing = 3$ mm). A complication that had to be tackled in the design of the magnetoacoustic system was capacitive and inductive interference from the signal generator to electrical PZT (lead zirconate titanate) ultrasound detectors. The experimental proof of second harmonic magnetoacoustic

signals appeared to be particularly challenging as it is not possible to generate alternating magnetic fields for magnetoacoustics without emitting also considerable RF harmonics. In order to isolate true magnetoacoustic signals from such interference signals, we based magnetoacoustic detection to a home-built π -phase shifted FBG (fiber-Bragg-grating) based interferometric sensor [23]. The FBG design is impervious to electromagnetic interference, offering correct magnetoacoustic detection. Data capture was performed in the frequency domain using a spectrum analyzer.

Magnetoacoustic experiments based on conducting objects.

We first investigated the presence of second harmonic magnetoacoustic responses using materials of high electric conductivity. Conducting objects dissipate significant thermal energy when exposed to AMFs due to induced circular currents (Eddy currents). A steel rod ($\varnothing = 2$ mm, 10 mm length) was placed within the Helmholtz coil in a water containing imaging tank (Fig. 1(b)) under RF induction at $f_{RF} = 820$ kHz. Experimental measurements in this case were performed in the presence and absence of the steel rod, employing a PZT transducer placed 30 mm from the location of the sample. The use of a PZT transducer in this study enabled the characterization of possible interference measurements. Measurements without the rod characterized interference coupling at the second harmonic of the RF wave $2f_{RF}$, establishing a baseline signal when using PZT-based detection (Fig. 1(d) - blue dotted curve). Introducing the conductive rod in the experimental arrangement gave rise to a magnetoacoustic response that is stronger than the baseline interference signal by 13.6 dB. This response was exactly at double the frequency of the magnetic excitation i.e. $f_{MA} = 2f_{RF} = 1.64$ MHz and exhibited a signal to noise ratio (SNR) of 61 dB (Fig. 1(d) - red curve).

Eq. (3) and Eq. (4) describe a quadratic increase of magnetoacoustic pressure with applied magnetic field H_0 . To confirm the true origin of the magnetoacoustic signal, we recorded the pressure as a function of linearly increasing B -field. As a result, we observed the expected quadratic response of the pressure as shown in the inset in (Fig. 1(d)), disproving the predictions of Ref. [18] and confirming Eq. (4).

Heating experiments.

Before investigating whether magnetic nanoparticles can generate magnetoacoustic signals, we first benchmarked the heating rate of various magnetic compounds (Fig. 2(a)). The hypothesis motivating the heating rate measurements is that nanoparticles with high specific loss power (SLP) will also efficiently generate magnetoacoustic signals. We particularly focused on commercially available magnetite particles (Fe_3O_4) with hydrodynamic diameters ranging from 30 - 200 nm, which are applied in clinical and preclinical imaging and therapy methodologies such as MRI, MPI, and magnetic hyperthermia [8, 37, 38]. The particles with

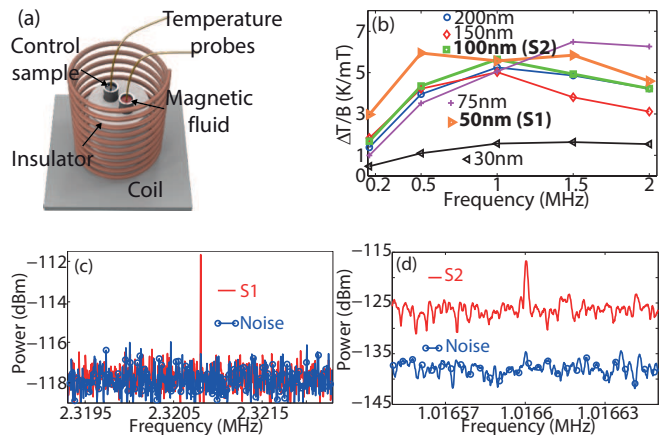


FIG. 2. Magnetic fluid heating and magnetoacoustic signal induction. (a) Schematic of temperature sensing using different nanoparticles. (b) Heating rates of 6 different magnetic fluids after 10 minute magnetic field exposure. The magnetic field-normalized temperature increase is shown at 5 discrete frequency steps. (c) Magnetoacoustic sensing of magnetic nanoparticles using the interferometric ultrasound sensor. The red curve displays a magnetoacoustic signal from sample S1 at $f_{MA} = 2.3208$ MHz excited at $f_{RF} = 1.1604$ MHz. The blue dotted curve depicts the baseline measurement without coupling medium, confirming RF-interference free detection. (d) Magnetoacoustic sensing at $f_{RF} = 508.3$ kHz using sample S2. The red curve shows the magnetoacoustic response at $f_{MA} = 2f_{RF} = 1.0166$ MHz while the blue curve represents the RF-free baseline measurement when the interferometer is turned off.

a concentration of 25 mg ml^{-1} were placed within a solenoid (Figs. 1(a) and 2(a)) and exposed to CW excitation for 10 minutes. Temperatures were recorded using fiber based temperature sensors that are unaffected by radiofrequency interferences. Despite sophisticated water cooling of our induction coil, we experienced environmental heating of the nanoparticle specimens placed within the coil. To correct for heating of the samples we subtracted the temperature increase of a control specimen consisting of deionized water which was measured simultaneously (see Fig. 2(a)). Energy uptake is frequency dependent, therefore we repeated this measurement at 5 discrete frequencies $f_{RF} = 166$ kHz, 500 kHz, 1 MHz, 1.5 MHz, 2 MHz (Fig. 2(b)). We found that magnetite nanoparticles exhibit low absorption of magnetic fields at frequencies $f_{RF} < 500$ kHz and a relatively flat absorption profile for $500 \text{ kHz} < f_{RF} < 2$ MHz. While literature suggests iron-oxide nanoparticles with a particle size in the order of 9 - 15 nm for efficient heat generation [8, 39], we found that nanoparticles with a hydrodynamic size of $x_h = 30$ nm (Chemicell, Berlin), equivalent to a magnetic core size of $x_m = 12 - 17$ nm, exhibited lowest magnetic field absorption (Fig. 2(b), black curve). Highest heating rates of 6.49 K mT^{-1} however were achieved using 75 nm particles, equivalent to a magnetic core size

of $x_m = 63 - 67$ nm, at $f_{RF} = 1.5$ MHz. Particles ranging from $x_h = 50 - 200$ nm had a relatively flat absorption from 500 kHz to 2 MHz. As an example, the magnetite nanoparticle with $x_h = 100$ nm that we chose for subsequent experiments exhibited a field-normalized heating rate of $\Delta T = 4.35$ K mT $^{-1}$ at 500 kHz (Fig. 2(b)). Compared to other heat induction studies, this temperature increase corresponds to a relatively low specific loss power of $SLP = 248$ mJ (g s) $^{-1}$ [8].

Magnetoacoustic experiments using nanoparticles.

To investigate whether magnetic nanoparticles generate magnetoacoustic effects in response to CW excitation, we performed magnetoacoustic measurements of magnetic nanoparticles with different sizes and concentration filled in PVC-tubing. Sample S1 consisted of fluidMAG-D nanoparticles with $x_h = 50$ nm at a concentration of 100 mg ml $^{-1}$ while sample S2 comprised fluidMAG-D nanoparticles with $x_h = 100$ nm at 25 mg ml $^{-1}$ concentration. The PVC-specimens were placed in the magnetoacoustic system (Fig. 1(a)) and measured at different excitation frequencies using the optical US-sensor schematized in Fig. 1(c). Under magnetic field exposure at $f_{RF} = 1.1604$ MHz, we observed second harmonic acoustic signals from S1 at a frequency of $f_{MA} = 2.3208$ MHz, exhibiting SNR of 6 dB after 20 averages (Fig. 2(c), red line). To confirm the decoupling efficiency and to exclude the impact of interference on our acoustic sensor, we removed the acoustic coupling medium from the water tank, impeding acoustic wave propagation and revealing the noise floor level of the interferometric sensor (Fig. 2(c), blue dotted line). To confirm second harmonic acoustic signal generation at frequencies where the specific loss power of the nanoparticles is lower, we repeated this experiment substituting the specimen to S2 (fluidMAG-D, $x_h = 100$ nm) and changing the magnetic field to $f_{RF} = 508$ kHz. Similarly, we observed a magnetoacoustic signal at the expected frequency $f_{MA} = 1.016$ MHz, exhibiting a SNR of 8.7 dB after 10 averages (Fig. 2(d), red line). Disabling the interferometric sensor by powering off the laser unit (displayed in Fig. 1(c)) revealed the RF-free noise floor level of our ultrasound sensor (see Fig. 2(d), blue dotted line).

Magnetoacoustic experiments employing labeled cells.

Next, we interrogated whether it would be possible to detect magnetoacoustic responses when particles are taken up by cells. We studied heating rates and magnetoacoustic signals collected from the murine macrophage cell line ANA-1 incubated with different types of magnetic particles (see Supplemental Material [25]). Different batches of cells were prepared, whereby batch C1 comprised cells incubated with large nanoparticles ($x_h > 200$ nm), and C2 consisted of cells labeled with small sized nanoparticles ($x_h < 100$ nm).

Figure 3(a) shows the heating rate of labeled macrophages at $f_{RF} = 660$ kHz after subtracting

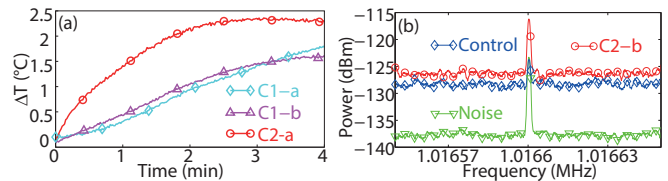


FIG. 3. Magnetoacoustic sensing of macrophages with nanoparticles. (a) Heating rates of ANA-1 cells loaded with magnetic particles C1-a (cyan diamond line), C1-b (purple triangle line), and C2-a (red dotted line) after subtraction of background heating. (b) Second harmonic acoustic response of ANA-1 cells incubated with fluidMAG-Amine (red dotted line). The control measurement of unlabeled ANA-1 cells (blue diamond line) and the noise measurement after disabling the optical sensor (green triangle line) show the non-linear EMI response of the RF amplifier.

the temperature increase of deionized water. As expected, the absorption rates of labeled macrophages are lower than heating experiments using bulk solutions at higher nanoparticle concentrations (Fig. 2(b)). The specific loss power was determined to be ~ 25 and 53 mJ (g s) $^{-1}$ for the C1, and C2 cell specimen, respectively. The two-fold SLP observed in cell batch C2 compared to batch C1 suggests that higher heating rates can be achieved using smaller diameter particles.

To interrogate whether magnetoacoustic signals could be detected from labeled cells, we employed macrophage cells labeled with small hydrodynamic core nanoparticles (C2-b, $x_h = 100$ nm, FluidMAG-Amine) which have shown strong heating in *in-vitro* experiments as demonstrated in Fig. 2(b). A control sample consisting of unlabeled ANA-1 cells was also measured. The frequency of the system was tuned to $f_{RF} = 508$ kHz and measurements were based on the interferometric detector to avoid interference signals. In a first measurement, displayed in Fig. 3(b) (red circle line), we observed the presence of magnetoacoustic waves from labeled cells at the predicted magnetoacoustic frequency $f_{MA} = 1.016$ MHz, exhibiting a SNR of ~ 10 dB after averaging 100 signals. Turning off the laser unit and disabling acoustic wave detection, we measured remnant interference possibly due to the metallic parts of the interferometric hardware itself. This interference signal is independent of ultrasound sensor position relatively to the specimen and exhibited a power level of $P_{RF} = -123.3$ dBm (Fig. 3(b), green triangle line), 7.1 dB below the magnetoacoustic signal. To exclude the possibility that unlabeled ANA-1 cells generate magnetoacoustic signals, we replaced the FluidMAG-Amine labeled cells with the ANA-1 cell control batch and recorded its magnetoacoustic response. In this setting illustrated in Fig. 3(b) (blue diamond line), no magnetoacoustic signal was measured. Instead, we observed a parasitic signal due to interference coupling with a power level of $P_{RF} = -123.6$ dBm, similar to

the previous measurement when the interferometric ultrasound sensor is disabled. This experiment confirmed magnetoacoustic signals from macrophages labeled with magnetic nanoparticles, exceeding interferences by more than 7 dB.

Discussion and Conclusion

In this work, we introduced magnetoacoustics, i.e. we theoretically and experimentally demonstrated the previous undocumented ability to detect pressure waves from magnetic nanoparticles placed within CW magnetic fields. Theoretically, we derived Eq. (4), which predicts the presence of second harmonic acoustic responses from magnetic particles and matter when excited with CW magnetic fields. To prove that such signals can be experimentally measured, we designed and implemented the first documented magnetoacoustic scanner. To minimize interference effects and conclusively interrogate the existence of magnetoacoustic signals, an optical interferometric sensor was employed, attaining a noise equivalent pressure of approximately 100 Pa over a bandwidth of 20 MHz [40] almost approaching the sensitivity of PZT based ultrasound sensors [41]. Similar optical detection has previously been applied in intravascular imaging [40] as well as for deep tissue imaging *in-vivo* [42] while magnetoacoustic imaging can be performed analogous to frequency-domain optoacoustics [43, 44]. Magnetoacoustic sensing demonstrated the existence of ultrasonic signals generated in response to sinusoidal AMFs. Contrary to former predictions that such signals cannot be generated, this observation proves the existence of magnetoacoustic responses. Magnetoacoustic signals are also expected in response to magnetic pulses. A characteristic however of the CW excitation is the appearance of only second harmonic responses. These

responses are expected at any frequency range; however frequencies around 1 MHz optimally match the range of magnetic energy absorption by common magnetic particles.

Tissues have very low ultrasound emission. Conventional thermoacoustic implementations using electrical pulses generate responses from the entire tissue absorbing electric energy due to conductivity [45–47]. In contrast, since no magnetic energy is deposited in tissues, only magnetic particles generate ultrasonic responses to AMFs. This basic feature, demonstrated by sensing labeled cells, leads to zero-background sensing of magnetic particles, in analogy to fluorescence or radio-isotope sensing. Magnetoacoustics can increase the specificity of magnetic particle detection and directly determine energy deposition in tissues, since acoustic responses are linearly related to the deposited energy density. This feature could be employed to characterize magnetic particles and determine their accumulation in tissues, for example as associated with magnetic hyperthermia studies. Likewise, when using known amounts of particles, magnetoacoustic sensing could be employed to spatiotemporally characterize magnetic fields.

We acknowledge financial support from the Alexander von Humboldt Foundation through a Feodor Lynen Research Fellowship, from the German Research Foundation (DFG) Research Grant (RO 4268/4 – 1), and support from the DFG Reinhart Koselleck award ‘High resolution near-field thermoacoustic sensing and imaging’ (NT 3/9 – 1).

Correspondence to: v.ntziachristos@tum.de, stephan.kellnberger@tum.de

-
- [1] R. Weissleder, M. Nahrendorf, and M. J. Pittet, *Nat Mater* **13**, 125 (2014).
 - [2] J. R. McCarthy, F. A. Jaffer, and R. Weissleder, *Small* **2**, 983 (2006).
 - [3] J. Huang, X. Zhong, L. Wang, L. Yang, and H. Mao, *Theranostics* **2**, 86 (2012).
 - [4] M. Mehrmohammadi, J. Oh, S. Mallidi, and S. Y. Emelianov, *Mol Imaging* **10**, 102 (2011).
 - [5] A. L. Oldenburg, J. R. Gunther, and S. A. Boppart, *Opt Lett* **30**, 747 (2005).
 - [6] B. Gleich and J. Weizenecker, *Nature* **435**, 1214 (2005).
 - [7] A. M. Derfus, G. von Maltzahn, T. J. Harris, T. Duza, K. S. Vecchio, E. Ruoslahti, and S. N. Bhatia, *Advanced Materials* **19**, 3932 (2007).
 - [8] J. H. Lee, J. T. Jang, J. S. Choi, S. H. Moon, S. H. Noh, J. W. Kim, J. G. Kim, I. S. Kim, K. I. Park, and J. Cheon, *Nature Nanotechnology* **6**, 418 (2011).
 - [9] T. O. Tasci, I. Vargel, A. Arat, E. Guzel, P. Korkusuz, and E. Atalar, *Medical Physics* **36**, 1906 (2009).
 - [10] S. Laurent, S. Dutz, U. O. Hafeli, and M. Mahmoudi, *Adv Colloid Interface Sci* **166**, 8 (2011).
 - [11] H. Huang, S. Delikanli, H. Zeng, D. M. Ferkey, and A. Pralle, *Nat Nanotechnol* **5**, 602 (2010).
 - [12] S. A. Stanley, J. E. Gagner, S. Damanpour, M. Yoshida, J. S. Dordick, and J. M. Friedman, *Science* **336**, 604 (2012).
 - [13] T. Knopfel and W. Akemann, *Nature Nanotechnology* **5**, 560 (2010).
 - [14] T. Y. Liu, S. H. Hu, D. M. Liu, S. Y. Chen, and I. W. Chen, *Nano Today* **4**, 52 (2009).
 - [15] B. P. Timko, K. Whitehead, W. W. Gao, D. S. Kohane, O. Farokhzad, D. Anderson, and R. Langer, *Annual Review of Materials Research*, Vol **41**, 1 (2011).
 - [16] V. Ntziachristos, *Nat Methods* **7**, 603 (2010).
 - [17] L. V. Wang and S. Hu, *Science* **335**, 1458 (2012).
 - [18] D. Piao, R. A. Towner, N. Smith, and W. R. Chen, *Med Phys* **40**, 063301 (2013).
 - [19] X. H. Feng, F. Gao, and Y. J. Zheng, *Applied Physics Letters* **103** (2013).
 - [20] X. Feng, F. Gao, R. Kishor, and Y. Zheng, *Sci Rep* **5**, 11489 (2015).
 - [21] M. S. Aliroteh, G. Scott, and A. Arbabian, *Electronics Letters* **50**, 790 (2014).
 - [22] S. Kellnberger, M. Omar, G. Sergiadis, and V. Ntzi-

- achristos, *Applied Physics Letters* **103** (2013).
- [23] A. Rosenthal, D. Razansky, and V. Ntziachristos, *Opt Lett* **36**, 1833 (2011).
- [24] R. E. Rosensweig, *Journal of Magnetism and Magnetic Materials* **252**, 370 (2002).
- [25] See Supplemental Material at [url], which includes Refs. [18,24,26-34], for further details.
- [26] P. W. Goodwill, G. C. Scott, P. P. Stang, and S. M. Conolly, *IEEE Trans Med Imaging* **28**, 1231 (2009).
- [27] M. Kallumadil, M. Tada, T. Nakagawa, M. Abe, P. Southern, and Q. A. Pankhurst, *Journal of Magnetism and Magnetic Materials* **321**, 1509 (2009).
- [28] Y. Kohl, G. J. Oostingh, A. Sossalla, A. Duschl, H. von Briesen, and H. Thielecke, *Nanoscale Res Lett* **6**, 505 (2011).
- [29] R. Ludwig, M. Stapf, S. Dutz, R. Muller, U. Teichgraber, and I. Hilger, *Nanoscale Res Lett* **9**, 602 (2014).
- [30] M. R. Loebinger, P. G. Kyrtatos, M. Turmaine, A. N. Price, Q. Pankhurst, M. F. Lythgoe, and S. M. Janes, *Cancer Res* **69**, 8862 (2009).
- [31] J. Riegler, A. Liew, S. O. Hynes, D. Ortega, T. O'Brien, R. M. Day, T. Richards, F. Sharif, Q. A. Pankhurst, and M. F. Lythgoe, *Biomaterials* **34**, 1987 (2013).
- [32] E. Kim, J. S. Oh, I. S. Ahn, K. I. Park, and J. H. Jang, *Biomaterials* **32**, 8654 (2011).
- [33] A. J. Cole, A. E. David, J. Wang, C. J. Galban, H. L. Hill, and V. C. Yang, *Biomaterials* **32**, 2183 (2011).
- [34] B. Perez-Lopez and A. Merkoci, *Advanced Functional Materials* **21**, 255 (2011).
- [35] D. Yoo, J. H. Lee, T. H. Shin, and J. Cheon, *Acc Chem Res* **44**, 863 (2011).
- [36] J. P. Fortin, C. Wilhelm, J. Servais, C. Menager, J. C. Bacri, and F. Gazeau, *J Am Chem Soc* **129**, 2628 (2007).
- [37] L. Xiao, J. Li, D. F. Brougham, E. K. Fox, N. Feliu, A. Bushmelev, A. Schmidt, N. Mertens, F. Kiessling, M. Valldor, B. Fadeel, and S. Mathur, *ACS Nano* **5**, 6315 (2011).
- [38] A. P. Khandhar, R. M. Ferguson, H. Arami, and K. M. Krishnan, *Biomaterials* **34**, 3837 (2013).
- [39] M. Gonzales-Weimuller, M. Zeisberger, and K. M. Krishnan, *Journal of Magnetism and Magnetic Materials* **321**, 1947 (2009).
- [40] A. Rosenthal, S. Kellnberger, D. Bozhko, A. Chekkoury, M. Omar, D. Razansky, and V. Ntziachristos, *Laser & Photonics Reviews* **8**, 450 (2014).
- [41] A. M. Winkler, K. Maslov, and L. V. Wang, *Journal of Biomedical Optics* **18** (2013).
- [42] A. P. Jathoul, J. Laufer, O. Ogunlade, B. Treeby, B. Cox, E. Zhang, P. Johnson, A. R. Pizzeby, B. Philip, T. Marafioti, M. F. Lythgoe, R. B. Pedley, M. A. Pule, and P. Beard, *Nature Photonics* **9**, 239 (2015).
- [43] P. Mohajerani, S. Kellnberger, and V. Ntziachristos, *Photoacoustics* **2**, 111 (2014).
- [44] S. Kellnberger, N. C. Deliolanis, D. Queiros, G. Sergiadis, and V. Ntziachristos, *Optics Letters* **37**, 3423 (2012).
- [45] R. A. Kruger, K. K. Kopecky, A. M. Aisen, D. R. Reinecke, G. A. Kruger, and J. Kiser, W. L., *Radiology* **211**, 275 (1999).
- [46] D. Razansky, S. Kellnberger, and V. Ntziachristos, *Med Phys* **37**, 4602 (2010).
- [47] S. Kellnberger, A. Hajiaboli, D. Razansky, and V. Ntziachristos, *Phys Med Biol* **56**, 3433 (2011).